Title: Monitoring land surface albedo and vegetation dynamics using high spatial and temporal resolution synthetic time series from Landsat and the MODIS BRDF/NBAR/albedo product

Authors: Zhuosen Wang[1,3*], Crystal B. Schaaf[2], Qingsong Sun[2], JiHyun Kim[4], Angela M. Erb[2], Feng Gao[5], Miguel O. Román[3], Yun Yang[5], Shelley Petroy[6], Jeffrey R. Taylor[7], Jeffrey G. Masek[3], Jeffrey T. Morisette[8], Xiaoyang Zhang[9], Shirley A. Papuga[10]

Affiliations:

[1]Earth System Science Interdisciplinary Center, University of Maryland College Park, College Park, MD, USA

[2]School for the Environment, University of Massachusetts Boston, Boston, MA, USA.

[3]NASA Goddard Space Flight Center, Greenbelt, MD, USA.

[4]Department of Geography, Indiana University Bloomington, Bloomington, IN, USA.

[5] USDA, Agricultural Research Service, Hydrology and Remote Sensing Laboratory, Beltsville, MD, USA

[6]National Ecological Observatory Network, Boulder, CO, USA.

[7]Institute of Technology Campus, Nova Scotia Community College, Halifax, NS, Canada

[8]U.S. Geological Survey, Department of the Interior North Central Climate Science Center, Fort Collins, CO, USA

[9]Geospatial Sciences Center of Excellence, South Dakota State University, Brookings, SD, USA.

[10]School of Natural Resources and the Environment, University of Arizona, Tucson, Arizona, USA.

*Correspondence to: zhuosen.wang@nasa.gov

Key words: Albedo; Vegetation Index; Data Fusion; Phenology; Remote sensing

Key points:

1. Synthetic time series of albedo and EVI can capture land surface dynamics with high similarity to tower and field data.
2. The RMSE and bias of the synthetic albedo values are less than 0.013 and within $\pm$ 0.006, respectively as compared to Ameiflux field data
3. In the future access to spatially representative NEON tower albedometer data will greatly improve our ability to evaluate moderate resolution satellite products.

Abstract:

Seasonal vegetation phenology can significantly alter surface albedo which in turn affects the global energy balance and the albedo warming/cooling feedbacks that impact climate change. To monitor and quantify the surface dynamics of heterogeneous landscapes, high temporal and spatial resolution synthetic time series of albedo and the enhanced vegetation index (EVI) were generated from the 500 m Moderate Resolution Imaging Spectroradiometer (MODIS) operational Collection V006 daily BRDF/NBAR/albedo products and 30 m Landsat 5 albedo and near-nadir reflectance data through the use of the Spatial and Temporal Adaptive Reflectance Fusion Model (STARFM). The traditional Landsat Albedo (Shuai et al., 2011) makes use of the MODIS BRDF/Albedo products (MCD43) by assigning appropriate BRDFs from coincident MODIS products to each Landsat image to generate a 30 m Landsat albedo product for that acquisition date. The available cloud free Landsat 5 albedos (due to clouds, generated every 16 days at best) were used in conjunction with the daily MODIS albedos to determine the appropriate 30 m albedos for the intervening daily time steps in this study. These enhanced daily 30 m spatial resolution synthetic time series were then used to track albedo and vegetation phenology dynamics over three Ameriflux tower sites (Harvard Forest in 2007, Santa Rita in 2011 and Walker Branch in 2005). These Ameriflux sites were chosen as they are all quite nearby new towers coming on line for the National Ecological Observatory Network (NEON), and thus represent locations which will be served by spatially paired albedo measures in the near future. The availability of data from the NEON towers will greatly expand the sources of tower albedometer data available for evaluation of satellite products. At these three Ameriflux tower sites the synthetic time series of broadband shortwave albedos were evaluated using the tower albedo measurements with a Root Mean Square Error (RMSE) less than 0.013 and a bias within the range of ± 0.006. These synthetic time series provide much greater spatial detail than the 500 m gridded MODIS data, especially over more heterogeneous surfaces, which improves the efforts to characterize and monitor the spatial variation across species and communities. The mean of the difference between maximum and minimum synthetic time series of albedo within the MODIS pixels over a subset of satellite data of Harvard Forest (16 km by 14 km) was as high as 0.2 during the snow-covered period and reduced to around 0.1 during the snow-free period. Similarly, we have used STARFM to also couple MODIS Nadir BRDF Adjusted Reflectances

(NBAR) values with Landsat 5 reflectances to generate daily synthetic times series of NBAR and thus Enhanced Vegetation Index (NBAR-EVI) at a 30 m resolution. While normally STARFM is used with directional reflectances, the use of the view angle corrected daily MODIS NBAR values will provide more consistent time series. These synthetic times series of EVI are shown to capture seasonal vegetation dynamics with finer spatial and temporal details, especially over heterogeneous land surfaces.

1. Introduction

Global surface temperatures have increased by approximately 0.6^{o}C in the past three decades (Hansen et al., 2010, 2006). This warming has contributed to a lengthening of the terrestrial vegetation growing season, especially in the mid- and high latitudes (Körner and Basler, 2010; Menzel and Fabian, 1999; Menzel et al., 2006; Myneni et al., 1997). Changes in the timing of leaf-out impact essential ecosystem processes; therefore accurate monitoring of phenology is required to understand the variability in terrestrial ecosystem change (Baldocchi et al., 2001; Churkina et al., 2005; Cleland et al., 2006; Piao et al., 2007; Richardson et al., 2012, 2009).

Land surface albedo plays a crucial role in land surface climate and biosphere models as a key climate forcing variable (Dirmeyer and Shukla, 1994; Hall, 2004; Lofgren, 1995; Ollinger et al., 2008). Typical surface albedo can range from as high as 0.8 over a pure snow-covered area to as low as 0.1 over vegetation during the snow-free period(Jin et al., 2002). This suggests that climate-driven changes in phenology (e.g. the onset of spring and snowmelt) may result in significant changes in the surface albedo. At lower albedo, the surface absorbs more solar energy and increases the local surface temperature which in turn affects the timing of phenological events (Richardson et al., 2013). This surface albedo feedback loop perpetuates further warming and climate change.

Trend analysis of vegetation albedo and phenology has been previously carried out using the high temporal resolution 500 m gridded MODIS albedo and Nadir Bidirectional Reflectance Distribution Function (BRDF)-Adjusted Reflectance (NBAR)-derived Vegetation Indices (VI) (Friedl et al., 2014; Ganguly et al., 2010; Zhang et al., 2003)]. The MODIS 500 m

BRDF/NBAR/albedo product (MCD43A) (Schaaf, 2008; Schaaf et al., 2011, 2002) provides high quality surface reflectance anisotropy retrievals over a variety of land surface types with high accuracy (Jin et al., 2003; Liang et al., 2002; Liu et al., 2009; Román et al., 2010, 2009; Wang et al., 2012, 2014). MODIS NBAR (MCD43A4) standardizes the MODIS directional reflectances to a nadir view at the illumination of local solar noon to eliminate the angular effect on the biophysical related parameters.

However, there are limitations to the application of daily 500 m gridded MODIS products such as NBAR and albedo in highly heterogeneous landscapes. Snow cover over different land types within a single MODIS pixel may melt at different rates and the vegetation green-up within a coarse satellite pixel of a mixed land cover type is usually dominated by the proportion of vegetation with the earlier green-up times (Zhang et al., 2017). As such, enhanced high resolution temporal and spatial data are critical to enable more detailed phenological monitoring (Liang et al., 2014). A persistent issue with current remotely sensed data is that sensors capture either high spatial resolution and low temporal resolution (e.g. Landsat, ASTER) or coarser spatial resolution and higher temporal resolution (e.g. MODIS, VIIRS). This limits the ability to monitor rapid land surface processes, particularly in heterogeneous landscapes. Several algorithms have been developed to blend these two resolutions of datasets to generate high temporal and spatial resolution surface reflectance (Emelyanova et al., 2013; Gao et al., 2006; Hilker et al., 2009; Roy et al., 2008; Zhu et al., 2010; Zurita-Milla et al., 2009). The Spatial and Temporal Adaptive Reflectance Fusion Model (STARFM) (Gao et al., 2006) has been successfully applied to generate high spatial and temporal resolution reflectance time series by combining cloud-free Landsat and MODIS reflectance data for vegetation monitoring. In this study, the STARFM algorithm is utilized to produce high spatial and temporal resolution albedo and VI time series by fusing Landsat and MODIS data.

Essential in the development of accurate satellite-driven remotely sensed products is the need for ground validation over various land covers, temporal scales, and seasonal dynamics over the long-term. In order to examine the ability of long-term field and tower networks such as Ameriflux and specifically the new National Ecological Observation Network (NEON) to provide *in situ* reference data for MODIS and other moderate resolution satellite sensors, we

present here an analysis of the spatial representativeness of the 20 core NEON terrestrial tower sites and thus their suitability to serve as moderate resolution albedo evaluation sites. NEON is a comprehensive observatory network designed to monitor physical and chemical properties of climate-related processes, including airborne remote sensing measurements, over the U.S. continental-scale ecosystem (Kampe, 2010; Keller et al., 2008). NEON sites are designed and sited to obtain accurate flux measurements, but the tower locations for other tower-based measurements such as albedo are not necessarily well suited for the evaluation of coarse resolution satellite acquisitions. Thus the STARFM method is used to generate synthetic high resolution albedo as well as NBAR-based vegetation indices at several select Ameriflux sites that are in close proximity to core NEON sites. This is done both to further demonstrate the enhancement that coupled MODIS-Landsat data products (including albedo and NBAR) provide for the detection of land surface characteristics and to illustrate the value of the increasingly available NEON tower data for satellite product validation over a wide range of ecosystems.

Thus the objectives of this study are to investigate the representativeness of tower measurements from NEON for the validation of moderate spatial resolution albedo products (e.g. MODIS, VIIRS) and demonstrate the concept of improving the ability to monitor temporal vegetation variations at the landscape scale especially heterogeneous surface by using STARFM to generate high temporal (daily) and spatial (30m) resolution albedo and NBAR-derived vegetation indices from the Collection V006 MODIS BRDF/NBAR/albedo products and Landsat 5 data.

2. Material and methodology

2.1 Study area and ground measurements

NEON consists of 47 terrestrial tower sites located across 20 eco-climatic domains in the US with one “core site” at each domain. Each of the 20 core terrestrial sites (Fig. 1) represents a different ecosystem region with varying vegetation types and climates (Hamilton et al., 2007; Kampe, 2010; Schimel et al., 2007). Long-term (30 year) data acquisition from NEON will provide site-based field ecological and climatic observations which can be coupled with regional and national-scale airborne remote sensing observations to describe land use and climate-driven seasonal change. The NEON network is currently under construction (with only nine sites starting to be operational), therefore we selected three Ameriflux tower sites (Harvard Forest,

Santa Rita and Walker Branch) (Table 1) which are located very close to NEON sites. These Ameriflux sites have the same land cover type as their NEON counterparts and the distances between the NEON and Ameriflux tower pairs are less than 0.8 km in all cases. The AmeriFlux network, established by the Department of Energy (DOE), provides ecosystem level exchanges of CO_2, water, and energy (including surface albedo) (Law et al., 2002; Running et al., 1999). In this study the Ameriflux tower measurements were used to evaluate the daily high spatial resolution synthetic time series of albedo. The Harvard Forest site is a mixed deciduous broadleaf and evergreen needleleaf forest dominated by red maple (*Acer rubrum*), red oak (*Quercus rubra*), birch (*Betula*), and hemlock (*Tsuga canadensis*). The Walker Branch site is near the NEON Oak Ridge site and is a 50-year-old broadleaf forest stand dominated by oak (*Quercus alba L., Q. prinus L.*), hickory (*Carya ovata(Mill.) K. Koch*), maple (*Acer rubrum L., A. saccharum*), and tulip poplar (*Liriodendron tulipifera L.*). Both of these Ameriflux towers are mounted with Kipp and Zonen albedometers and radiometers to measure shortwave albedo. The Santa Rita Creosote site is located near the NEON Santa Rita Experimental Range site. This open shrub site is dominated by creosote bush (*Larrea tridentata*) and the shortwave albedo is derived from a Kipp and Zonen four component radiometer (Sanchez-Mejia and Papuga, 2014; Sanchez-Mejia et al., 2014). The local noon ground albedo is calculated as the ratio of upwelling radiation and downwelling radiation. In addition, field measurements of green-up dates with full bud break were obtained at the Harvard Forest site through the long-term ecological research (LTER) network database (http://www.lternet.edu/sites/hfr) (Richardson and O'Keefe, 2009; Zhang et al., 2006). Phenocam photos acquired at Santa Rita Creosote site were used to track the vegetation dynamics.

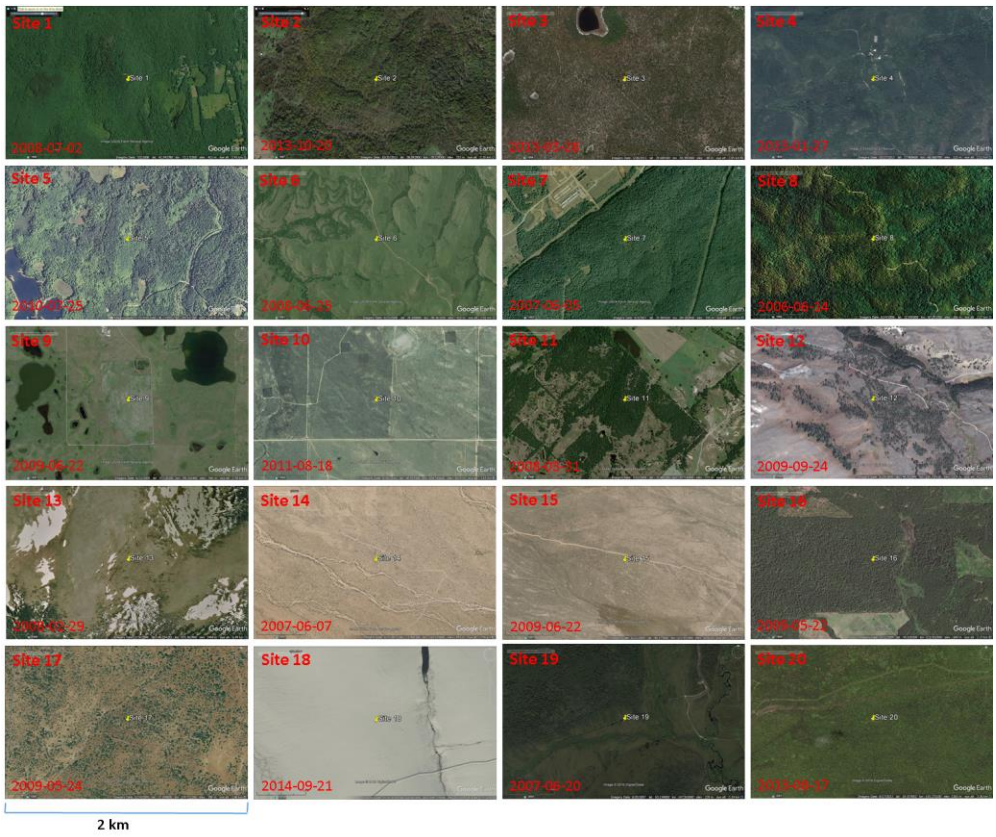

196

197 Fig. 1 Landscapes and acquired dates of the 20 NEON core sites (from Google Earth).

198

199 Table 1: Characteristics of the three Ameriflux and 20 NEON tower sites in 20 NEON domains

Domain Number	Site Name	Network	Latitude/Longitude	State	Land type	Tower height (m)
D01	Harvard Forest	NEON	42.5369/-72.1727	Massachusetts	Mixed Forest	36
D01	Harvard Forest	Ameriflux	42.54378/-72.1715	Massachusetts	Mixed Forest	30
D02	Smithsonian Conservation Biology Institute	NEON	38.8929/-78.1395	Virginia	Deciduous broadleaf forest	50
D03	Ordway-Swisher Biological Station	NEON	29.6893/-81.9934	Florida	Evergreen broadleaf forest	33
D04	Guanica Forest	NEON	17.9696/-66.8687	Puerto Rico	Evergreen broadleaf forest	20
D05	University of Notre Dame Environmental	NEON	46.2339/-89.5373	Michigan	Mixed forest	36

	Research Center					
D06	Konza Prairie Biological Station	NEON	39.1008/-96.5631	Kansas	Prairie	8
D07	Oak Ridge	NEON	35.9641/-84.2826	Tennessee	Deciduous broadleaf forest	38
D07	Walker Branch	Ameriflux	35.9588/-84.2874	Tennessee	Deciduous broadleaf forest	44
D08	Talladega National Forest	NEON	32.9505/-87.3933	Alabama	Mixed forest	35
D09	Woodworth	NEON	47.1282/-99.2414	North Dakota	Grass	8
D10	Central Plains Experimental Range	NEON	40.8155/-104.7456	Colorado	grass	8
D11	LBJ National Grassland	NEON	33.4012/-97.5700	Texas	Deciduous broadleaf forest	22
D12	Yellowstone Northern Range (Frog Rock)	NEON	44.9535/-110.5391	Wyoming	Evergreen needleleaf forest	20
D13	Niwot Ridge Mountain Research Station	NEON	40.0543/-105.5824	Colorado	grass	8
D14	Santa Rita Experimental Range	NEON	31.9107/-110.8355	Arizona	shrub	8
D14	Santa Rita Creosote	Ameriflux	31.9083/-110.8396	Arizona	shrub	2.75
D15	Onaqui-Ault	NEON	40.1776/-112.4524	Utah	sagebrush steppe	8
D16	Wind River Experimental Forest	NEON	45.8205/-121.9519	Washington	Evergreen needleleaf forest	86
D17	San Joaquin Experimental Range	NEON	37.1088/-119.7323	California	open woodland	36
D18	Toolik Lake	NEON	68.6611/-149.3705	Alaska	tundra	8
D19	Caribou Creek - Poker Flats Watershed	NEON	65.1540/-147.5026	Alaska	Evergreen needleleaf forest	18
D20	Upper Waiakea Forest Reserve	NEON	19.5577/-155.2711	Hawaii	Evergreen broadleaf forest	20

2.2 Satellite Data

The 500 m Collection V006 MODIS BRDF/NBAR/albedo product (MCD43) and the 30 m Landsat 5 surface reflectance were used for this synthetic study. The MODIS BRDF/NBAR/albedo product makes use of a linear "kernel-driven" RossThick-LiSparse Reciprocal (RTLSR) BRDF model which has been shown to be well suited to describe the reflectance anisotropy of each pixel at a 500-m gridded resolution over a variety of land covers (Lucht et al., 2000; Privette et al., 1997; Schaaf et al., 2002). In the past this multi-day product was retrieved every 8 days which limited its ability to capture rapidly changing land surface events such as vegetation emergence and snowmelt. However, the Collection V006 MODIS BRDF/albedo product, currently in production, is now retrieved daily and represents the best possible BRDF based on 16 days of input information. The day of interest is heavily weighted within the algorithm to allow daily monitoring of land surface change phenomena (Schaaf et al., 2011; Shuai et al., 2013; Wang et al., 2012).

The 30 m spatial resolution Landsat 5 surface reflectance over the three sites is derived from Landsat Ecosystem Disturbance Adaptive Processing System (LEDAPS) (Masek et al., 2006). The Landsat narrowband to broadband coefficients were applied to generate the shortwave broadband surface reflectance (He et al., 2014; Shuai et al., 2014). Landsat shortwave albedo is calculated from the Anisotropic Reflectance Factor (ARF) taken from a high quality MODIS pixel associated with the same spectral cluster (Shuai et al., 2011; Wang et al., 2012). The Shuai et al. (2011) (the so-called concurrent "MODIS-era" approach) uses an unsupervised classifier to cluster the individual scene-based multi-spectral Landsat data into ten to fifteen clusters, with the assumption that each cluster in the scene has similar instantaneous anisotropy features. The cluster map is reprojected from UTM to the MODIS sinusoidal projection and MODIS representative pixels that are relatively homogenous on the Landsat scale are identified. The ratio of the albedo-to-reflectance generated from the representative MODIS pixels BRDF which are associated with each Landsat cluster is then calculated to derive a Landsat albedo from the Landsat near nadir reflectance (at view angles ±7.5° from nadir) using equation (1).

$$A = (a/r(\Omega_l)) \cdot r_l \quad (1)$$

Where A is Landsat albedo to be calculated, r_l is observed Landsat reflectance and Ω_l is viewing and solar geometry of Landsat data. a is albedo and $r(\Omega_l)$ is the reflectance at Landsat sun view geometry. Both a and $r(\Omega_l)$ are derived by the BRDF parameters.

The cloud-free blue-sky shortwave broadband albedo (the actual bi-hemispherical reflectance) is derived by combining the synthetic shortwave Black-Sky Albedo (BSA) at local solar noon and the White-Sky Albedo (WSA) with a consideration of the diffuse and direct incident radiation at a specific time (Eq. 2) (Lewis and Barnsley, 1994; Román et al., 2010).

$$\alpha_{blue-sky}(\theta_i) = f_{diffuse}(\theta_i)\alpha_{white-sky} + (1 - f_{diffuse}(\theta_i))\alpha_{black-sky}(\theta_i) \quad (2)$$

Where $f_{diffuse}(\theta_i)$ is the proportion of diffuse irradiation at a specific solar zenith angle θ_i; the $f_{diffuse}$ is derived from AOD acquired from the MODIS aerosol product (MOD08).

Compared to the Normalized Difference Vegetation Index (NDVI) which can become saturated in dense vegetation, the Enhanced Vegetation Index (EVI) (Huete et al., 2002) improves sensitivity in high biomass regions and is used to derive the MODIS phenology product (Zhang et al., 2003). As such, the NBAR-derived EVI time series data are used to detect vegetation phenology metrics in this study.

2.3 The synthetic time series of shortwave broadband albedo and vegetation index

The STARFM algorithm is used to derive the synthetic time series of daily albedo and enhanced vegetation index at a 30m spatial resolution. STARFM blends the Landsat and MODIS data by using the spatially and temporally weighted difference between paired MODIS and Landsat pixels from same day images to predict intermediate values on MODIS dates and create a comprehensive phenological record (Gao et al., 2006). In this study both the synthetic daily shortwave broadband albedo and the EVI values were generated utilizing STARFM from the paired images of Landsat and MODIS albedo and the paired images of NBAR-derived EVI to model the non-linear change over the entire period (Emelyanova et al., 2013). STARFM is applied directly to the shortwave broadband albedo and EVI values rather than the underlying surface reflectance in order to reduce the mismatch in bandwidths between the Landsat and MODIS data. The daily MODIS NBAR-derived EVI (Collection V006) and Landsat EVI are fused to build EVI time-series for deriving the vegetation phenology. Daily 30 m spatial

resolution STARFM images were generated for the entire year of 2007at Harvard Forest, Santa Rita in 2011 and Walker Branch in 2005. The spatial extent of STARFM images is 16 km by 14 km at Harvard Forest and 5 km by 5 km at both the Santa Rita and Walker Branch sites. To facilitate a more robust analysis of the surface heterogeneity, a larger plot was selected for statistics at the Harvard Forest site (16 km by 14 km). This was done to include most of land classes of typical forested areas of the northeastern United States (evergreen forest, deciduous forest, grassland, inland water bodies and residential areas). The cloud, cloud shadow and snow flags created by the LEDAPS algorithm were applied to select clear sky snow-free Landsat 5 TM images prior to processing in STARFM (Table 2).

The phenology metrics (e.g. onset of vegetation green-up) were retrieved by applying the piecewise logistic function to the synthetic time series snow-free daily EVI (Zhang et al., 2003). No further smoothing processes was performed over the synthetic time series data before fitting the piecewise logistic function.

Table 2. The acquisition dates of Landsat 5 TM images used for the Harvard Forest, Walker Branch, and Santa Rita sites

Site	Harvard Forest (year-month-day)	Walker Branch (year-month-day)	Santa Rita (year-month-day)
Landsat 5 TM Data	2007-02-11 2007-03-30 2008-04-18* 2007-06-19 2007-09-07	2005-02-22 2005-03-10 2005-05-13 2005-09-18 2005-10-04 2005-10-20	2011-01-13 2011-01-29 2011-02-14 2011-03-02 2011-03-18 2011-04-03 2011-05-21 2011-06-22 2011-10-12 2011-10-28

* Landsat obtained from 2008-04-18 is utilized for the spring period as there was no available cloud free imagery in 2007 and no disturbance/change between year 2007 and 2008.

2.4 Surface heterogeneity analysis

The heterogeneity of the Enhanced Vegetation Index (EVI) and shortwave broadband blue sky albedo is analyzed by considering the standard deviation (Eq. 3) and difference between the

maximum and minimum values (Eq. 4) within the moderate grid (480 m) using the 30 m STARFM synthetic datasets. Recognizing that the actual grid size of the so-called "500 m" MODIS gridded product is 463 m, in this study the analysis is performed for each 480 m grid (16 by 16 Landsat pixels) within the subsets of the three sites.

$$Y_{480m-stdv} = \sqrt{(\sum_{i=1}^{N}(\bar{x}_{30m} - x_{i_{30m}})^2)/(N-1)} \quad (3)$$

$$Y_{480m-diff} = x_{max(30m)} - x_{min(30m)} \quad (4)$$

$$\bar{Z}_{480m} = (\sum_{j=1}^{M} Y_{j_{480m}})/M \quad (5)$$

Where x refers to vegetation index or shortwave broadband blue sky albedo at 30 m spatial resolution. *N* is the total number of 30 m clear sky pixels within each 480 m grid. *M* is the number of 480 m grids within the study area. $Y_{480m\text{-}stdv}$ and $Y_{480m\text{-}diff}$ are the standard deviation and difference of the maximum and minimum values within the 480m grid respectively. $\bar{Z}_{480m}$ is the mean value of standard deviation ($Y_{480m\text{-}stdv}$) or difference of maximum and minimum ($Y_{480m\text{-}diff}$) values within the study area. These measures reflect the degrees of heterogeneity within a MODIS pixel from Landsat pixel resolution

The heterogeneity and spatial representativeness of the NEON sites were also analyzed using a semivariogram analysis (Carroll and Cressie, 1996; Matheron, 1963). The semivariogram is one of the most efficient tools to reveal the spatial variability of land surfaces and describe the surface heterogeneity and spatial representativeness (Román et al., 2009; Woodcock et al., 1988a, 1988b). Albedo spatial representativeness analysis was performed using semivariograms created from the 30 m Landsat data to evaluate the surface heterogeneity of the regions around the 20 NEON core ground towers (Román et al., 2009; Wang et al., 2014, 2012). The spatial representativeness of the ground measurements for moderate spatial resolution satellite products (e.g. MODIS, VIIRS) is evaluated at each NEON site. Although gridded as a 500 m product, the MCD43A BRDF/albedo/NBAR products are generated from multi-angular surface reflectance observations with varied footprints. As such, it is difficult to determine the exact footprint of one MODIS gridded albedo pixel. Campagnolo et al. (2016) showed that the effective spatial

resolution of 500 m gridded MODIS BRDF/albedo/ NBAR product at mid latitudes is around 833 m by 618 m. Therefore, we analyzed the spatial representativeness of each site based on a conservatively larger area. The ground measurements can be used to appropriately evaluate moderate spatial resolution remote sensing products if the surface is spatially homogenous within the larger area. The variogram estimator is fitted to a spherical model to derive spatial attributes (range, sill and nugget effect). The scale requirement index (R_{se}) (Eq. 6) (Román et al., 2009) derived from the semivariogram analysis measures the relative spatial variation in albedo considering both the footprint of the ground instrument and the surrounding landscape. The surface is spatially representative with respect to the MODIS footprint when the R_{se} is less than 0.243 (Román et al., 2009).

$$R_{se} = \exp\left[-\sqrt{(g/a_x)^2 + (g/a_{1.5x})^2}\right]; x = 1.0km \quad (6)$$

Where:

$$g = 2H\tan(FOV) \quad (7)$$

a is the range of two Landsat subsets of sizes x and $1.5x$; H is the height of the field albedometer; FOV[degrees] is the half field-of-view of the albedometer; g is the footprint of ground albedo measurements. The site is spatially representative when $g >= a_x$ and $g >= a_{1.5x.}$ so that the Rse values are between [0.0, $e^{-\sqrt{2}} \approx 0.243$].

The sill is the ordinate value of the range at which the variogram levels off to an asymptote and describes the maximum semivariance. Smaller sill values indicate less variation in albedo and a more homogenous surface. Note that the spatially representative analysis is only applicable to moderate resolution satellite measurements such as albedo and in no way reflects the suitability of the site as a flux tower. Spatially representative analysis is not necessarily required to validate fine spatial resolution satellite products (e.g. Landsat) as the footprints of the tower measurements are larger than the Landsat pixel size.

3. Results and Discussion

3.1 Land surface heterogeneity

The temporal standard deviation and difference of maximum and minimum shortwave broadband blue sky albedo and EVI over a 16 km by 14 km area at the Harvard Forest site

computed using Eq. (1-4) is shown in Fig. 2. The spatial extent of this subset is the same as that shown in Fig. 5 with the Ameriflux flux tower located at the center. The land cover of this area includes evergreen forest, deciduous forest, grassland, several inland water bodies and residential areas. As shown in Fig. 2, albedo is more heterogeneous during the snow-covered period with the highest albedo values over completely snow-covered surfaces and relatively low albedo over the forested areas where complete snow cover is rare. The maximum albedo within the study area is 0.9 while the minimum albedo is less than 0.1. The mean of the difference between maximum and minimum albedo over the entire study area is around 0.2 during the snow-covered period and reduced to around 0.1 during the snow-free period. The standard deviation of the albedo measurements shows similar trends to the mean of the difference between maximum and minimum albedo. The mean albedo standard deviation is at around 0.014 during the snow-free period and increases to 0.05 during the snow-covered period. EVI is relatively homogeneous during the dormant period and more heterogeneous during the growing season due to the different land cover growth patterns. The mean of the difference between maximum and minimum EVI over the study area is around 0.35 during the growing season; which is about 0.1 higher than the dormant period. The mean EVI standard deviation during the growing season is about 0.02 higher than the values during the dormant period.

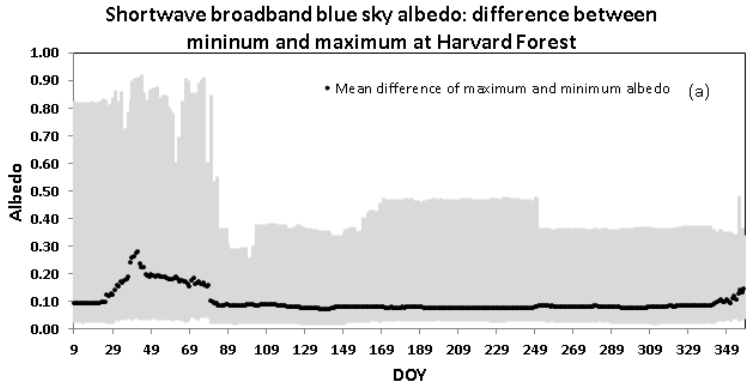

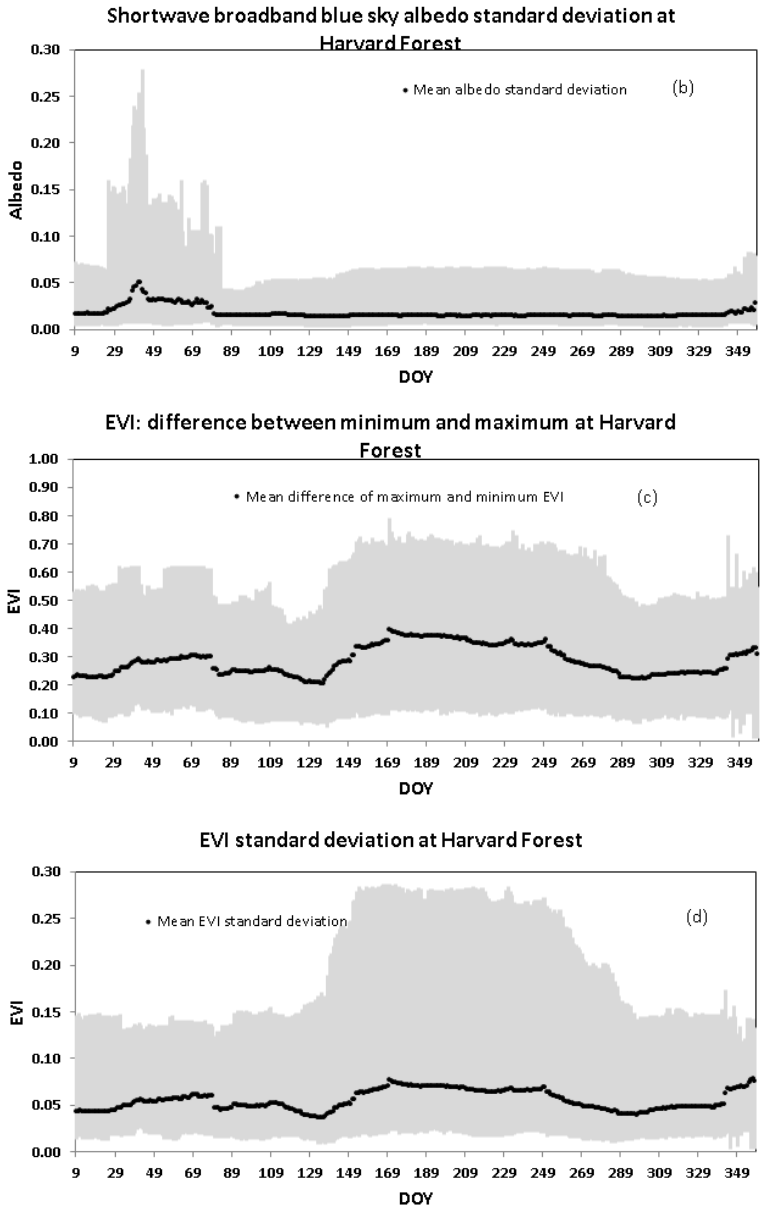

Fig. 2. Temporal plot showing the difference of the maximum and minimum (a) and the standard deviation (b) of shortwave broadband blue sky albedo within the 480 m spatial resolution grids based on 30 m synthetic albedo times series at the Harvard Forest in 2007; Temporal plot of the difference of the maximum and minimum (c) and the standard deviation (d) of EVI within 480 m spatial resolution pixels based on 30 m synthetic EVI time series at the Harvard Forest in 2007. The subset area is 16 km by 14 km. The gray area represents the range of maximum and minimum values within the study area.

The big ranges in the standard deviation and maximum and minimum difference of both albedo and EVI indicate that there is significant spatial variation in the land surface of the Harvard Forest at MODIS pixel scales. Therefore, fine spatial resolution data is required to accurately quantify the effects of vegetation changes on the terrestrial carbon cycle and climate change at the patch-scale (Goward et al., 2008; Masek et al., 2013; Shuai et al., 2011).

Here we investigate the representativeness of the albedos that will be measured from NEON towers for the validation of the MODIS albedo product based on the surface heterogeneity and spatial representativeness analysis (Fig. 3). While this analysis focuses on the MODIS albedo product, the results are applicable to other satellite products with similar spatial resolutions (e.g. VIIRS). Most of the NEON core terrestrial sites with tower height higher than 10m are relatively homogenous and the ground measured albedo is spatially representative of the MODIS albedo during both the leaf-on and leaf-off seasons (Table 3). Although the R_{se} values of all the 8 m tower sites are larger than 0.243, the sill values of Konza Prairie Biological Station, Central Plains Experimental Range, Santa Rita Experimental Range, Toolik Lake and 20m tower height Guanica Forest, Yellowstone Northern Range and Upper Waiakea Forest Reserve sites are low at less than 0.0005. These sites can also be considered homogenous and representative. Fig. 4 shows that the difference between MODIS and ground measured albedo at the Santa Rita site is less than 0.02. The Caribou Creek taiga, Woodworth, LBJ National Grassland, and Niwot Ridge Mountain Research Station sites represent grassland and forest ecotones and are particularly heterogeneous and may not serve as ideal validation sites for moderate resolution satellite products. In general, shrub and open woodland sites, located in areas with little human activity and no water bodies nearby, are all spatially representative. It should be noted that just as the location of the NEON core towers has been optimized for flux measurements, the actual height of the towers and the placement of the downward radiometers has also been optimized for flux measurements and is governed by the height of the surrounding canopy. Although sites located in heterogenous regions (e.g. the Caribou Creek taiga) are not spatially representative for moderate spatial resolution albedo validation, the footprints of these tower albedo are typically larger than a single pixel of high spatial resolution albedo (e.g. Landsat, Sentinel 2). As such, these sites can still be used to evaluate the accuracy of higher spatial resolution albedo products.

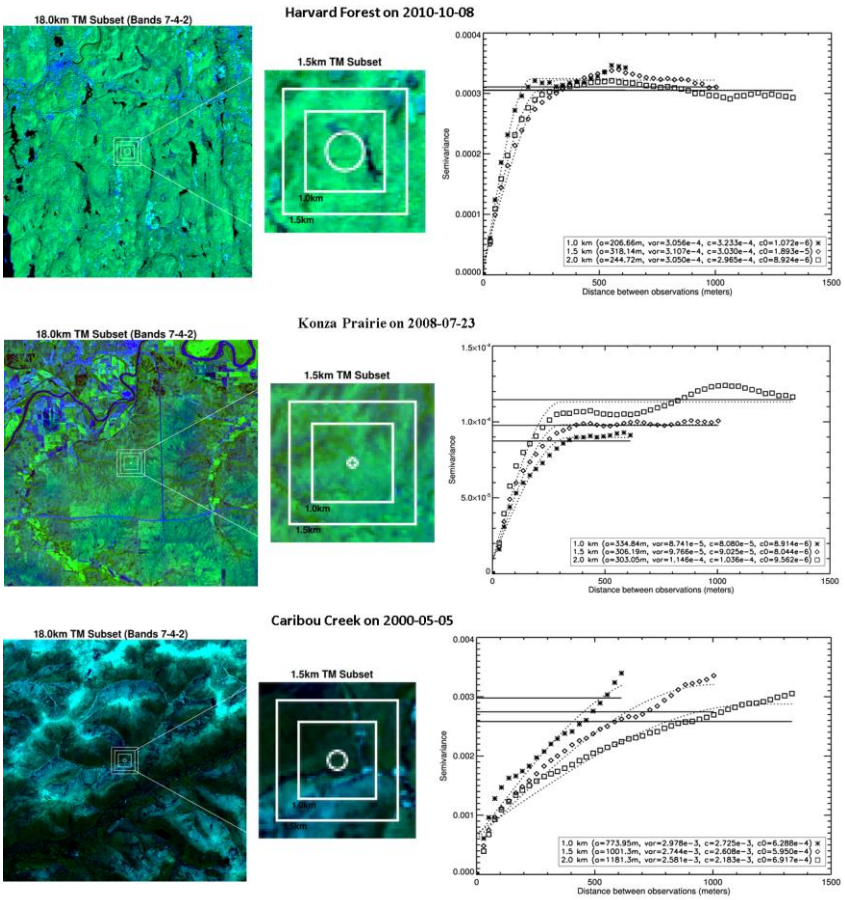

Fig. 3 Shortwave reflectance composite (TM Bands 7–4–2) and corresponding semivariogram functions, variogram estimator (points), spherical model (dotted curves), and sample variance (solid straight lines) using regions of 1.0 km (asterisks), 1.5 km (diamonds), and 2.0 km (squares), centered over Harvard Forest on 2010-10-08, Konza Prairie on 2008-07-23, Caribou Creek - Poker Flats Watershed on 2000-05-05. The circles show the footprint of tower albedo measurements calculated from the tower height and albedometer FOV.

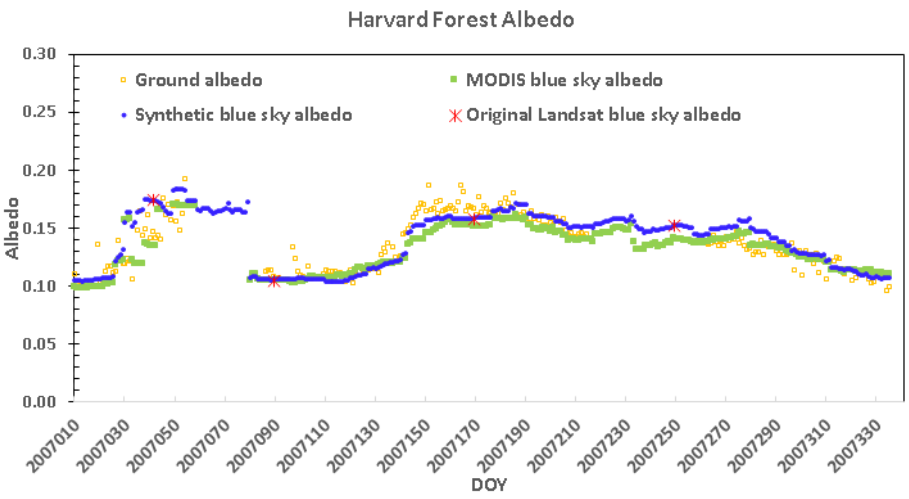

421

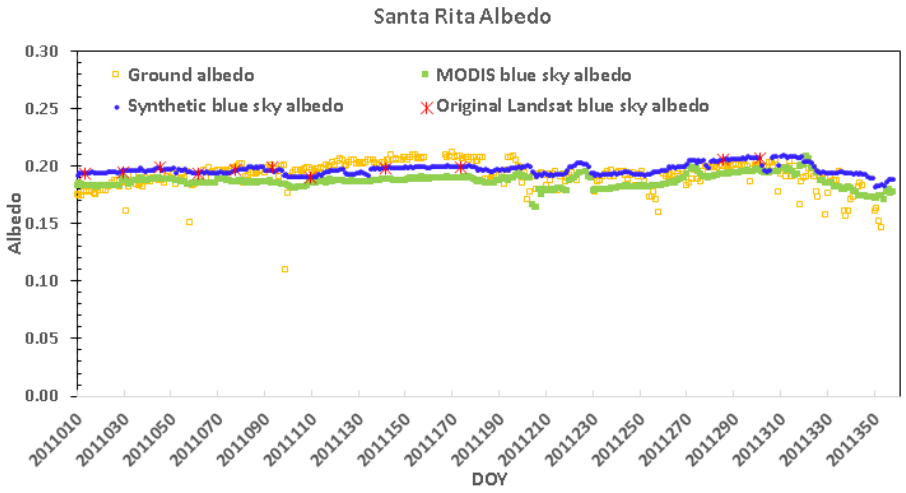

422

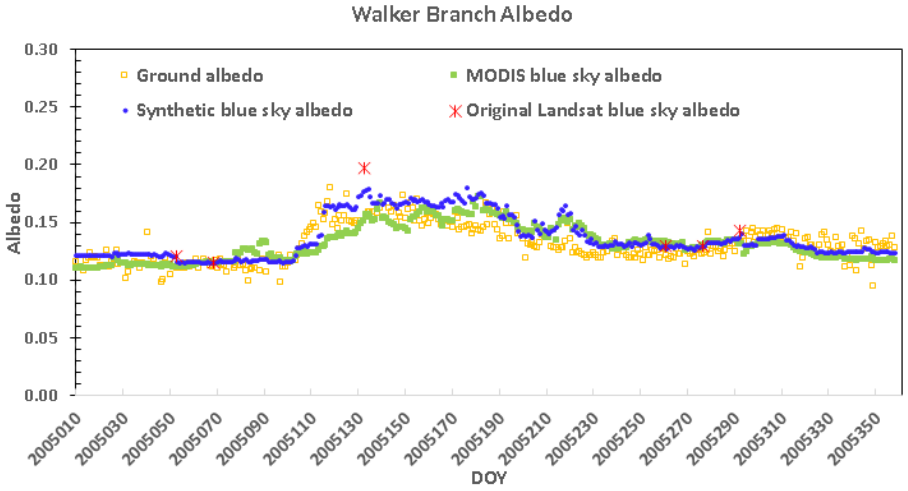

423
424

425 Fig. 4. Comparison of synthetic time series of blue-sky albedo with ground-measured
426 albedo, MODIS blue-sky albedo, and Landsat blue-sky albedo over Harvard Forest
427 (2007), Santa Rita (2011), and Walker Branch (2005) sites. Synthetic, ground-measured,

and MODIS albedo measurements were obtained on a daily basis. Landsat 5 measurements were derived from all cloud-free images available in each year (Table 2)

Table 3. Spatial representativeness status of NEON sites for moderate spatial resolution satellite albedo product validation. The highest "sill" values of the three analyzed spatial regions sites (1.0 km, 1.5 km and 2.0 km) in the semivariogram analysis are presented here.

Domain Number	Site Name	R_{se}		Sill	
		Leaf on	Leaf off	Leaf on	Leaf off
D01	Harvard Forest	0.0726	0.2104	0.0003	0.0003
D02	Smithsonian Conservation Biology Institute	0.0148	0.0253	0.0001	0.0002
D03	Ordway-Swisher Biological Station	0.0618	N/A[§]	0.0003	N/A
D04	Guanica Forest	0.2705	N/A	0.0001	N/A
D05	University of Notre Dame Environmental Research Center	0.1408	0.0673	0.0011	0.0004
D06	Konza Prairie Biological Station	0.6395	0.6531	0.0001	0.0005
D07	Oak Ridge	0.0469	0.1777	0.0003	0.0006
D08	Talladega National Forest	0.0341	N/A	0.0001	N/A
D09	Woodworth	0.5626	0.5738	0.0014	0.0011
D10	Central Plains Experimental Range	N/A	N/A	0.0002	0.0002
D11	LBJ National Grassland	N/A	N/A	0.0005	0.0015
D12	Yellowstone Northern Range (Frog Rock)	0.5222	0.5209	0.0004	0.0004
D13	Niwot Ridge Mountain Research Station	0.5970	0.7196	0.0004	0.0011
D14	Santa Rita Experimental Range	N/A	N/A	0.0002	0.0002
D15	Onaqui-Ault	0.5873	0.5365	0.0001	0.0002

D16	Wind River Experimental Forest	0.0085	N/A	0.0007	N/A
D17	San Joaquin Experimental Range	0.0393	0.0636	0.0001	0.0003
D18	Toolik Lake	N/A	N/A	0.0002	
D19	Caribou Creek - Poker Flats Watershed	N/A	N/A	0.0008	0.0034
D20	Upper Waiakea Forest Reserve	0.4609	N/A	0.0001	N/A

[§]N/A represents data not available (evergreen vegetation sites for leaf off (site 3, 4, 16, 19, and 20), no clear sky images available (site 8), or sites where the semivariogram curve fails to fit the spherical model (site 10, 11, 14, 18, and 19)).

3.2 Synthetic shortwave albedo and EVI for land surface dynamics monitoring

The synthetic times series of 30 m broadband shortwave blue sky albedo is averaged according to the footprint of the tower albedometer for comparison with ground measurements. The albedos at Harvard Forest are around 0.19 during winter as snow beneath the forest canopy increases reflectance. The albedo decreases with the snowmelt and then increases to a maximum of about 0.16 during the course of the growing season (Fig. 4). Gaps in the data record are a result of missing ground albedo measurements from DOY 55 to 84 at the Harvard forest tower. The MODIS and synthetic albedo were not retrieved from around the Harvard Forest tower from DOY 59 to 79 due to the lack of valid MODIS reflectance data. Unsurprisingly, the synthetic 30 m albedo time series captures finer spatial characteristics than the MODIS data alone while maintaining similar seasonal dynamics (Fig. 5). The Santa Rita site is relatively stable with albedos remaining near 0.2 all year (appropriate for such a semiarid open shrub land site). The seasonal dynamics at this site are mainly dominated by the change of soil moisture (Sanchez-Mejia et al., 2014). Walker Branch is a deciduous forest site with no winter snow cover. As such, the albedo is lower than Harvard Forest in the winter (~0.12) and increases to a maximum of 0.17 during the growing season. The RMSEs of the synthetic blue sky albedo as compared to the tower albedo values are 0.013, 0.009 and 0.012 for the Harvard Forest, Santa Rita and Walker Branch sites respectively and the biases for the three sites are 0.002, 0.003 and 0.006 respectively. The footprint of the tower albedo measurements is close (Santa Rita) to or larger than (Harvard Forest and Walker Branch) the 30 m Landsat and synthetic albedo pixel sizes, yet

smaller than the effective spatial resolution of MODIS albedo. Landsat and synthetic albedo values were averaged according to the tower footprints for comparison, as such the area mismatch between combined Landsat and synthetic pixels and the ground footprint is less than the mismatch between ground footprint and a MODIS pixel. As a result, the Landsat and synthetic albedo values are slightly closer to the tower albedos than the MODIS albedo values (Fig. 4) over the three sites. The RMSE of the more homogenous shrub land (Santa Rita) is lower than the values at forest sites (Harvard Forest and Walker Branch). The combined accuracy of the synthetic blue sky albedo at these all three sites (RMSE 0.016, bias −0.013) is close to the values in Shuai et al. (2011) and meets the absolute accuracy requirement of 0.02–0.05 (Sellers et al., 1995) required by modelers. The accuracy of the synthetic time series of blue sky albedo values is affected by the number and quality of the finer spatial resolution data. For example, only one Landsat image is available during the growing season (2005-05-13) at Walker Branch and this Landsat albedo value is 0.04 higher than the measured ground albedo. This observation is close to the edge of a cloud and is potentially contaminated by a thin cloud not detected with the Landsat cloud mask. Enhanced temporal resolution coverage of finer scale satellite data over these sites would obviously improve the synthetic time series results. The availability and improved technical capabilities (1.38μm cirrus band and the improved radiometric resolution) of Landsat 8 (2013) and Sentinel-2A (2015) obviously will contribute significantly to improved fine scale synthetic time series results. The synthetic 30 m albedo show a wider data range than the stand-alone MODIS albedo. This is because spatial details captured at the Landsat 30 m resolution are mixed/smoothed at the MODIS 500 m resolution. However, the number of original clear sky Landsat 5 observations is very limited at the Harvard Forest and Walker Branch sites with only four at Harvard Forest in 2007 and six at Walker Branch in 2005. The Santa Rita site, in a semiarid area, had 11 original clear sky Landsat 5 observations in 2011 (Table 2). However, in all cases, the daily synthetic EVI and albedo time series significantly expand the spatial and temporal resolution of datasets for climate study.

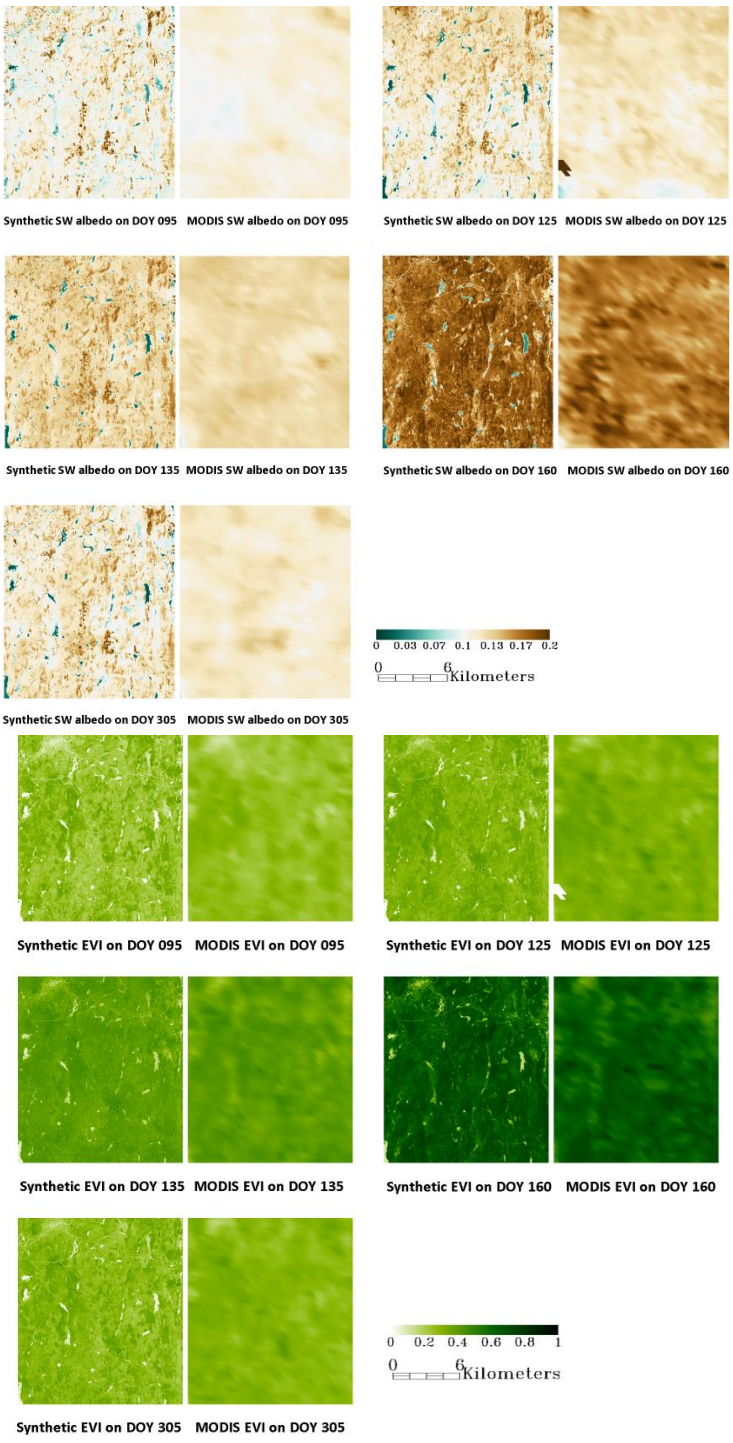

Fig. 5. The synthetic time series and MODIS shortwave broadband blue sky albedo and EVI at Harvard Forest subset (16 km by 14 km) on DOY 95, 125, 135, 160 and 305 in 2007.

The phenological metrics derived from multi-day composite datasets can mask high-frequency vegetation changes (Ju et al., 2010; McKellip et al., 2005; Narasimhan and Stow, 2010). Shuai et al. (2013) showed that subtle details in growth stages can be captured from daily MODIS NBAR-derived EVI. Currently the temporal resolution of the Landsat data makes it difficult to capture vegetation phenological metrics, particularly in the shoulder seasons (e.g. green-up, senescence) which are important in analyzing the impacts of climate change. The MODIS-Landsat derived synthetic daily 30 m spatial resolution times series of EVI can be used to monitor complex land surface characteristics, especially rapidly changing seasonal dynamics. The phenology patterns of the vegetation were well captured by the synthetic EVI time series at Harvard Forest in 2007 (Fig. 5; Fig. 6). The logistic model fitted EVI dates agrees well with the synthetic temporal EVI dates. The ground phenology information at Harvard Forest was measured every 4 days during the green-up period. In 2007, the green-up date determined from the synthetic 30 m data sets (Day Of Year (DOY) 120) matches well with the field measured date (124). The green-up date derived from 500 m MODIS product (MCD12Q2) (Zhang et al., 2003) was considerably earlier at DOY 115. The difference in the onset of green-up within a single MODIS pixel can be more than 10 days over the same forest type (Fig. 6b). This spatial variation in phenology could be caused by species distribution or small scale microclimates. Small scale microclimates have previously been shown to result in large phenological variability within hundreds of meters (Klosterman et al., 2014; Vitasse et al., 2009). The temporal variation of synthetic EVI times series however, captures the development of foliage stages at the Santa Rita site (Fig. 6c). The shrubs started to green-up on DOY 220 and reached the first peak on DOY 230 and the second peak on DOY 260 in 2011. The single year analysis in this study demonstrate an ability to derive temporal vegetation variations at high spatial resolution using a variety of data fusion techniques. Further work is required for different vegetation types over a longer period to extend this study to completely assess the implication of land surface heterogeneity on the phenological analyses.

The synthetic EVI also shows greater spatial detail than the MODIS EVI, especially over more heterogeneous surfaces. This improves our ability to characterize spatial variations in EVI across species and communities. The maximum EVI standard deviation within a 480 m grid at Harvard Forest is over 0.25 and the difference of maximum and minimum EVI within the 480 m grid can

be as high as 0.7 during the growing season (Fig. 2). In addition, the boundaries between forest types and water bodies are very clear in the synthetic EVI but difficult to identify in the MODIS EVI.

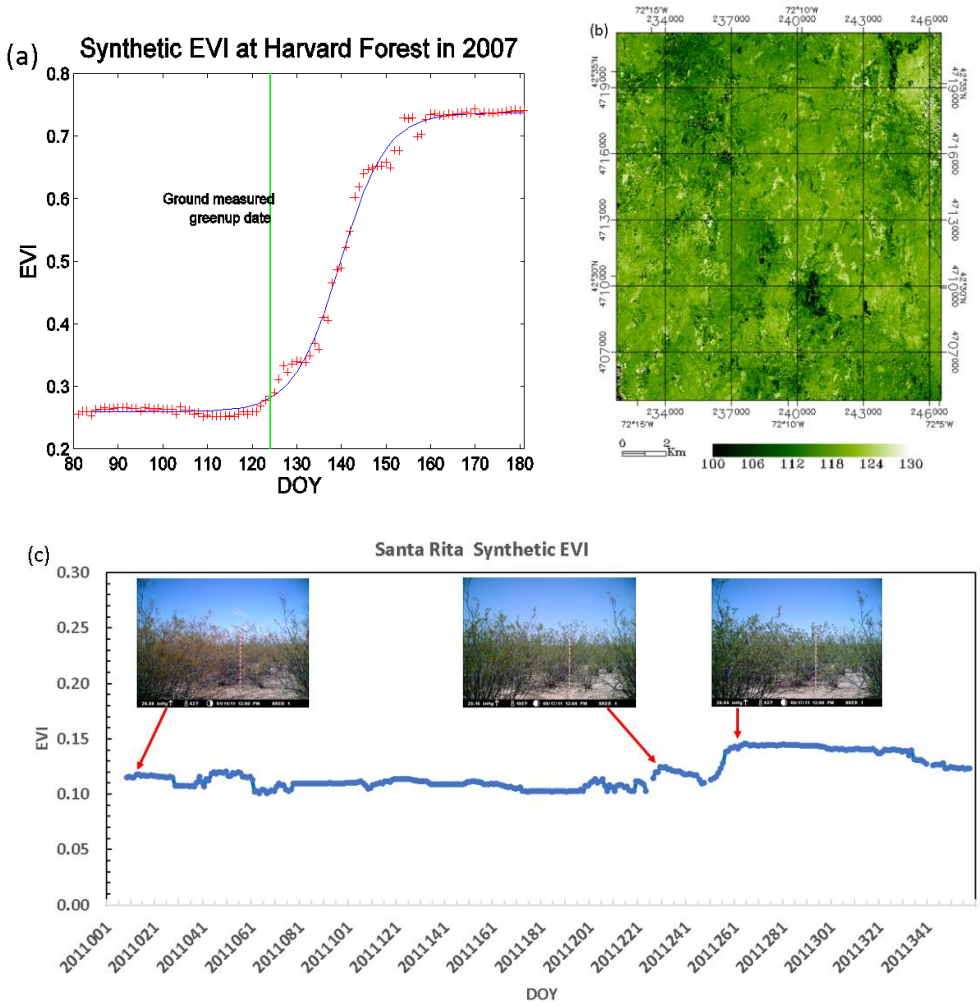

Fig. 6. (a) Temporal plot of synthetic time series EVI (red +) and logistic model fit (blue line) at Harvard Forest flux tower in 2007, (b) the onset (DOY) of green-up at Harvard Forest subset (16 km by 14 km) and (c) the temporal plot of synthetic EVI and phenocam photos at Santa Rita site.

4. Conclusion

The MODIS-Landsat coupled synthetic albedo and EVI times series are able to capture the land surface dynamics at high spatial resolution. Such a capability lays the ground work for long-term monitoring of vegetation phenology at the stand scale in response to climate change,

disturbance regimes, and other drivers. The heterogeneity analyses of all of the NEON sites and of the three Ameriflux sites used in this study indicates that the range of EVI and albedo within moderate spatial resolution grids is very large and higher spatial resolution vegetation index and albedo values are necessary to understand how individual vegetation types are responding to environmental forcing. The daily high spatial resolution synthetic vegetation index time series enhances the monitoring of vegetation phenology change. At the Harvard Forest site, the difference between the synthetic EVI determinations and the ground measured green-up date is within 4 days. This suggests that over mixed deciduous broadleaf and evergreen needleleaf forest ecosystems, the modeled phenology can be used to capture vegetation temporal variations at the landscape scale. The synthetic albedo time series match well with the ground albedo values with RMSE and bias less than 0.013 and within ± 0.006 respectively over the three Ameriflux sites. As more of the spatially representative NEON core site towers are established, continued comparisons and validation can be done to monitor seasonal and temporal trends. The establishment of the NEON core sites will contribute significantly to our knowledge of a diversity of ecosystems and provide key validation measurements for both satellite data and future models and simulations. However, as noted, the NEON sites were originally selected for applicability to serve as flux sites and not necessarily the best placements to evaluate satellite products, and therefore, this analysis of spatial representativeness is important in defining the appropriate usage of these NEON data. The observations of higher resolution surface phenology and energy change from the synthetic time series data will be continued with the newer generation of satellites including Landsat 8 Operational Land Imager (OLI), Sentinel-2A/B MultiSpectral Instrument (MSI), and Suomi-NPP Visible Infrared Imager Radiometer Suite (VIIRS) satellite sensors.

Acknowledgement

The Landsat data were downloaded from the USGS Earth Resources Observation and Science (EROS) Center Science Processing Architecture (ESPA) (https://espa.cr.usgs.gov). MODIS data were obtained from the NASA's Earth Observing System Data and Information System (EOSDIS) (http://reverb.echo.nasa.gov). Field albedo measurements were downloaded from AmeriFlux website (http://ameriflux.lbl.gov/). We gratefully acknowledge Dr. Tilden Meyers

from NOAA for providing ground albedo measurements at Walker Branch site, Dr. David Fitzjarrald from State University of New York at Albany for providing Harvard Forest ground albedo measurements and John O'Keefe from Harvard University for providing ground measured phenology data at Harvard Forest. This research was supported by NASA award [grant number NNX14A173G], Harvard Forest NSF LTER grant [grant number DEB-1237491] and NSF CAREER Award [grant number EAR-1255013]. Any use of trade, product, or firm names is for descriptive purposes only and does not imply endorsement by the U.S. Government.

Reference:

Baldocchi, D., Falge, E., Wilson, K., 2001. A spectral analysis of biosphere – atmosphere trace gas flux densities and meteorological variables across hour to multi-year time scales. Agric. For. Meteorol. 107, 1–27. doi:10.1016/S0168-1923(00)00228-8

Campagnolo, M.L., Sun, Q., Liu, Y., Schaaf, C., Wang, Z., Román, M.O., 2016. Estimating the effective spatial resolution of the operational BRDF, albedo, and nadir reflectance products from MODIS and VIIRS. Remote Sens. Environ. 175, 52–64. doi:10.1016/j.rse.2015.12.033

Carroll, S.S., Cressie, N., 1996. A comparison of geostatistical methodologies used to estimate snow water equivalent. Water Resour. Bull. 32, 267–278. doi:10.1111/j.1752-1688.1996.tb03450.x

Churkina, G., Schimel, D., Braswell, B.H., Xiao, X.M., 2005. Spatial analysis of growing season length control over net ecosystem exchange. Glob. Chang. Biol.

Cleland, E.E., Chiariello, N.R., Loarie, S.R., Mooney, H.A., Field, C.B., 2006. Diverse responses of phenology to global changes in a grassland ecosystem. Proc. Natl. Acad. Sci. U. S. A. 103, 13740–13744.

Dirmeyer, P.A., Shukla, J., 1994. Albedo as a modulator of climate response to tropical deforestation. J. Geophys. Res. 99, 20863–20877.

Emelyanova, I. V., McVicar, T.R., Van Niel, T.G., Li, L.T., van Dijk, A.I.J.M., 2013. Assessing the accuracy of blending Landsat–MODIS surface reflectances in two landscapes with contrasting spatial and temporal dynamics: A framework for algorithm selection. Remote Sens. Environ. 133, 193–209. doi:10.1016/j.rse.2013.02.007

Friedl, M. a, Gray, J.M., Melaas, E.K., Richardson, A.D., Hufkens, K., Keenan, T.F., Bailey, A., O'Keefe, J., 2014. A tale of two springs: using recent climate anomalies to characterize the sensitivity of temperate forest phenology to climate change. Environ. Res. Lett. 9, 054006. doi:10.1088/1748-9326/9/5/054006

Ganguly, S., Friedl, M. a., Tan, B., Zhang, X., Verma, M., 2010. Land surface phenology from MODIS: Characterization of the Collection 5 global land cover dynamics product. Remote Sens. Environ. 114, 1805–1816. doi:10.1016/j.rse.2010.04.005

Gao, F., Masek, J., Schwaller, M., Hall, F., 2006. On the blending of the Landsat and MODIS surface reflectance: predicting daily Landsat surface reflectance. IEEE Trans. Geosci. Remote Sens. 44, 2207–2218. doi:10.1109/TGRS.2006.872081

610 Goward, S.N., Masek, J.G., Cohen, W., Moisen, G., Collatz, G.J., Healey, S., Houghton, R. a.,
611 Huang, C., Kennedy, R., Law, B., Powell, S., Turner, D., Wulder, M. a., 2008. Forest
612 Disturbance and North American Carbon Flux. Eos, Trans. Am. Geophys. Union 89, 105.
613 doi:10.1029/2008EO110001

614 Hall, A., 2004. The Role of Surface Albedo Feedback in Climate. J. Clim. 17, 1550–1568.
615 doi:10.1175/1520-0442(2004)017<1550:TROSAF>2.0.CO;2

616 Hamilton, M.P., Graham, E. a., Rundel, P.W., Allen, M.F., Kaiser, W., Hansen, M.H., Estrin,
617 D.L., 2007. New Approaches in Embedded Networked Sensing for Terrestrial Ecological
618 Observatories. Environ. Eng. Sci. 24, 192–204. doi:10.1089/ees.2006.0045

619 Hansen, J., Ruedy, R., Sato, M., Lo, K., 2010. Global Surface Temperature Change. Rev.
620 Geophys. 48, 1–29. doi:10.1029/2010RG000345.1.INTRODUCTION

621 Hansen, J., Sato, M., Ruedy, R., Lo, K., Lea, D.W., Medina-elizade, M., 2006. Global
622 temperature change. Proc. Natl. Acad. Sci. U. S. A. 103, 14288–14293.

623 He, T., Liang, S., Wang, D., Shuai, Y., Yu, Y., 2014. Fusion of satellite land surface albedo
624 products across scales using a multiresolution tree method in the north central United States.
625 IEEE Trans. Geosci. Remote Sens. 52, 3428–3439. doi:10.1109/TGRS.2013.2272935

626 Hilker, T., Wulder, M. a., Coops, N.C., Seitz, N., White, J.C., Gao, F., Masek, J.G., Stenhouse,
627 G., 2009. Generation of dense time series synthetic Landsat data through data blending with
628 MODIS using a spatial and temporal adaptive reflectance fusion model. Remote Sens.
629 Environ. 113, 1988–1999. doi:10.1016/j.rse.2009.05.011

630 Huete, A., Didan, K., Miura, T., Rodriguez, E.P., Gao, X., Ferreira, L.G., 2002. Overview of the
631 radiometric and biophysical performance of the MODIS vegetation indices. Remote Sens.
632 Environ. 83, 195–213. doi:10.1016/S0034-4257(02)00096-2

633 Jin, Y., Schaaf, C.B., Gao, F., Li, X., Strahler, A.H., 2003. Consistency of MODIS surface
634 bidirectional reflectance distribution function and albedo retrievals: 1. Algorithm
635 performance. J. Geophys. Res. 108.

636 Jin, Y.B.S., Gao, F., Li, X., Strahler, A.H., Zeng, X., Dickinson, R.E., 2002. How does snow
637 impact the albedo of vegetated land surfaces as analyzed with MODIS data? Geophys. Res.
638 Lett. 29, 12–15. doi:10.1029/2001GL014132

639 Ju, J., Roy, D.P., Shuai, Y., Schaaf, C., 2010. Development of an approach for generation of
640 temporally complete daily nadir MODIS reflectance time series. Remote Sens. Environ.
641 114, 1–20. doi:10.1016/j.rse.2009.05.022

642 Kampe, T.U., 2010. NEON: the first continental-scale ecological observatory with airborne
643 remote sensing of vegetation canopy biochemistry and structure. J. Appl. Remote Sens. 4,
644 043510. doi:10.1117/1.3361375

645 Keller, M., Schimel, D.S., Hargrove, W.W., Hoffman, F.M., 2008. A continental strategy for the
646 National Ecological Observatory Network. Front. Ecol. Environ. 6, 282–284.
647 doi:10.1890/1540-9295(2008)6[282:ACSFTN]2.0.CO;2

648 Klosterman, S.T., Hufkens, K., Gray, J.M., Melaas, E., Sonnentag, O., Lavine, I., Mitchell, L.,
649 Norman, R., Friedl, M.A., Richardson, A.D., 2014. Evaluating remote sensing of deciduous
650 forest phenology at multiple spatial scales using PhenoCam imagery. Biogeosciences 11,
651 4305–4320. doi:10.5194/bg-11-4305-2014

Körner, C., Basler, D., 2010. Phenology Under Global Warming. Science (80-.). 327, 1461–1462. doi:10.1126/science.1186473

Law, B., Falge, E., Gu, L., Baldocchi, D., Bakwin, P., Berbigier, P., Davis, K., Dolman, A., Falk, M., Fuentes, J., 2002. Environmental controls over carbon dioxide and water vapor exchange of terrestrial vegetation. Agric. For. Meteorol. 113, 97–120. doi:10.1016/S0168-1923(02)00104-1

Lewis, P., Barnsley, M., 1994. Influence of the sky radiance distribution on various formulations of the earth surface albedo. Proc. Conf. Phys. Meas. Signatures Remote Sens.

Liang, L., Schwartz, M.D., Wang, Z., Gao, F., Schaaf, C.B., Tan, B., Morisette, J.T., Zhang, X., 2014. A Cross Comparison of Spatiotemporally Enhanced Springtime Phenological Measurements From Satellites and Ground in a Northern U.S. Mixed Forest. IEEE Trans. Geosci. Remote Sens. 52, 7513–7526. doi:10.1109/TGRS.2014.2313558

Liang, S., Fang, H., Chen, M., Shuey, C.J., Walthall, C., Daughtry, C., Morisette, J., Schaaf, C., Strahler, A., 2002. Validating MODIS land surface reflectance and albedo products: methods and preliminary results. Remote Sens. Environ. 83, 149–162. doi:10.1016/S0034-4257(02)00092-5

Liu, J., Schaaf, C., Strahler, A., Jiao, Z., Shuai, Y., Zhang, Q., Roman, M., Augustine, J. a., Dutton, E.G., 2009. Validation of Moderate Resolution Imaging Spectroradiometer (MODIS) albedo retrieval algorithm: Dependence of albedo on solar zenith angle. J. Geophys. Res. 114, D01106. doi:10.1029/2008JD009969

Lofgren, B., 1995. Surface albedo-climate feedback simulated using two-way coupling. J. Clim. 8, 2543–2562.

Lucht, W., Schaaf, C.B., Strahler, a. H., 2000. An algorithm for the retrieval of albedo from space using semiempirical BRDF models. IEEE Trans. Geosci. Remote Sens. 38, 977–998. doi:10.1109/36.841980

Masek, J.G., Goward, S.N., Kennedy, R.E., Cohen, W.B., Moisen, G.G., Schleeweis, K., Huang, C., 2013. United States Forest Disturbance Trends Observed Using Landsat Time Series. Ecosystems 16, 1087–1104. doi:10.1007/s10021-013-9669-9

Masek, J.G., Vermote, E.F., Saleous, N.E., Wolfe, R., Hall, F.G., Huemmrich, K.F., Gao, F., Kutler, J., Lim, T., 2006. A Landsat Surface Reflectance Dataset. IEEE Geosci. Remote Sens. Lett. 3, 68–72.

Matheron, G., 1963. Principles of geostatistics. Econ. Geol. 58, 1246–1266. doi:10.2113/gsecongeo.58.8.1246

McKellip, R., Ryan, R.E., Blonski, S., Prados, D., 2005. Crop surveillance demonstration using a near-daily MODIS derived vegetation index time series, in: Proceedings of the Third International Workshop on the Analysis of Multi-Temporal Remote Sensing Images 2005. pp. 54–58. doi:10.1109/AMTRSI.2005.1469839

Menzel, A., Fabian, P., 1999. Growing season extended in Europe. Nature 397, 659. doi:10.1038/311558a0

Menzel, A., Sparks, T.H., Estrella, N., Koch, E., Aasa, A., Ahas, R., Alm-Kubler, K., Bissolli, P., Braslavska, O., Briede, A., Chmielewski, F.M., Crepinsek, Z., Curnel, Y., Dahl, A., Defila, C., Donnelly, A., Filella, Y., Jatczak, K., Mage, F., Mestre, A., Nordli, O., Penuelas, J.,

694 Pirinen, P., Remisova, V., Scheifinger, H., Striz, M., Susnik, A., Viet, V., Arnold, J.H.,
695 Wielgolaski, F.-E., Zach, S., Zust, A., 2006. European phenological response to climate
696 change matches the warming pattern. Glob. Chang. Biol. 12, 1969–1976.

697 Myneni, R.B., Keeling, C.D., Tucker, C.J., Asrar, G., Nemani, R.R., 1997. Increased plant
698 growth in the northern high latitudes from 1981 to 1991. Nature 386, 698–702.

699 Narasimhan, R., Stow, D., 2010. Daily MODIS products for analyzing early season vegetation
700 dynamics across the North Slope of Alaska. Remote Sens. Environ. 114, 1251–1262.
701 doi:10.1016/j.rse.2010.01.017

702 Ollinger, S. V, Richardson, A.D., Martin, M.E., Hollinger, D.Y., Frolking, S.E., Reich, P.B.,
703 Plourde, L.C., Katul, G.G., Munger, J.W., Oren, R., Smith, M.L., Paw U, K.T., Bolstad, P.
704 V, Cook, B.D., Day, M.C., Martin, T.A., Monson, R.K., Schmid, H.P., 2008. Canopy
705 nitrogen, carbon assimilation, and albedo in temperate and boreal forests: Functional
706 relations and potential climate feedbacks. Proc. Natl. Acad. Sci. U. S. A. 105, 19336–
707 19341. doi:10.1073/pnas.0810021105

708 Piao, S., Friedlingstein, P., Ciais, P., Viovy, N., Demarty, J., 2007. Growing season extension
709 and its impact on terrestrial carbon cycle in the Northern Hemisphere over the past 2
710 decades. Global Biogeochem. Cycles 21, 1–11. doi:10.1029/2006GB002888

711 Privette, J.L., Eck, T.F., Deering, D.W., 1997. Estimating spectral albedo and nadir reflectance
712 through inversion of simple BRDF models with AVHRR/MODIS-Iike data. J. Geophys.
713 Res. 102, 29529–29542.

714 Richardson, A.D., Anderson, R.S., Arain, M.A., Barr, A.G., Bohrer, G., Chen, G., Chen, J.M.,
715 Ciais, P., Davis, K.J., Desai, A.R., Dietze, M.C., Dragoni, D., Garrity, S.R., Gough, C.M.,
716 Grant, R., Hollinger, D.Y., Margolis, H. a., McCaughey, H., Migliavacca, M., Monson,
717 R.K., Munger, J.W., Poulter, B., Raczka, B.M., Ricciuto, D.M., Sahoo, A.K., Schaefer, K.,
718 Tian, H., Vargas, R., Verbeeck, H., Xiao, J., Xue, Y., 2012. Terrestrial biosphere models
719 need better representation of vegetation phenology: results from the North American
720 Carbon Program Site Synthesis. Glob. Chang. Biol. 18, 566–584. doi:10.1111/j.1365-
721 2486.2011.02562.x

722 Richardson, A.D., Hollinger, D.Y., Dail, D.B., Lee, J.T., Munger, J.W., O'keefe, J., 2009.
723 Influence of spring phenology on seasonal and annual carbon balance in two contrasting
724 New England forests. Tree Physiol. 29, 321–331.

725 Richardson, A.D., Keenan, T.F., Migliavacca, M., Ryu, Y., Sonnentag, O., Toomey, M., 2013.
726 Climate change, phenology, and phenological control of vegetation feedbacks to the climate
727 system. Agric. For. Meteorol. 169, 156–173. doi:10.1016/j.agrformet.2012.09.012

728 Richardson, A.D., O'Keefe, J., 2009. Phenological differences between understory and overstory
729 a case study using the long-term Harvard Forest records, in: Phenology of Ecosystem
730 Processes: Applications in Global Change Research. pp. 87–117. doi:10.1007/978-1-4419-
731 0026-5_4

732 Román, M.O., Schaaf, C.B., Lewis, P., Gao, F., Anderson, G.P., Privette, J.L., Strahler, A.H.,
733 Woodcock, C.E., Barnsley, M., 2010. Assessing the coupling between surface albedo
734 derived from MODIS and the fraction of diffuse skylight over spatially-characterized
735 landscapes. Remote Sens. Environ. 114, 738–760. doi:10.1016/j.rse.2009.11.014

736 Román, M.O., Schaaf, C.B., Woodcock, C.E., Strahler, A.H., Yang, X., Braswell, R.H., Curtis,
737 P.S., Davis, K.J., Dragoni, D., Goulden, M.L., 2009. The MODIS (Collection V005)
738 BRDF/albedo product: Assessment of spatial representativeness over forested landscapes.
739 Remote Sens. Environ. 113, 2476–2498. doi:10.1016/j.rse.2009.07.009

740 Roy, D.P., Ju, J., Lewis, P., Schaaf, C., Gao, F., Hansen, M., Lindquist, E., 2008. Multi-temporal
741 MODIS–Landsat data fusion for relative radiometric normalization, gap filling, and
742 prediction of Landsat data. Remote Sens. Environ. 112, 3112–3130.
743 doi:10.1016/j.rse.2008.03.009

744 Running, S.W., Baldocchi, D.D., Turner, D.P., Gower, S.T., Bakwin, P.S., Hibbard, K.A., 1999.
745 A Global Terrestrial Monitoring Network Integrating Tower Fluxes, Flask Sampling,
746 Ecosystem Modeling and EOS Satellite Data. Remote Sens. Environ. 70, 108–127.
747 doi:10.1016/S0034-4257(99)00061-9

748 Sanchez-Mejia, Z.M., Papuga, S.A., 2014. Observations of a two-layer soil moisture influence
749 on surface energy dynamics and planetary boundary layer characteristics in a semiarid
750 shrubland. Water Resour. Res. 50, 306–317. doi:10.1002/2013WR014135

751 Sanchez-Mejia, Z.M., Papuga, S.A., Swetish, J.B., Van Leeuwen, W.J.D., Szutu, D., Hartfield,
752 K., 2014. Quantifying the influence of deep soil moisture on ecosystem albedo: The role of
753 vegetation. Water Resour. Res. 50, 4038–4053. doi:10.1002/2013WR014150

754 Schaaf, C.B., 2008. Albedo and Reflectance Anisotropy, Terrestrial Essential Climate Variables
755 for Climate Change Assessment, Mitigation and Adaptation, in: Sessa, R., Han, D. (Eds.),
756 GTOS-52. pp. 28–29.

757 Schaaf, C.B., Gao, F., Strahler, A.H., Lucht, W., Li, X., Tsang, T., Strugnell, N.C., Zhang, X.,
758 Jin, Y., Muller, J.-P., Lewis, P., Barnsley, M., Hobson, P., Disney, M., Roberts, G.,
759 Dunderdale, M., Doll, C., d'Entremont, R.P., Hu, B., Liang, S., Privette, J.L., Roy, D.,
760 2002. First operational BRDF, albedo nadir reflectance products from MODIS. Remote
761 Sens. Environ. 83, 135–148. doi:10.1016/S0034-4257(02)00091-3

762 Schaaf, C.B., Liu, J., Gao, F., Strahler, A.H., 2011. MODIS Albedo and Reflectance Anisotropy
763 Products from Aqua and Terra, in: B. Ramachandran, C. Justice, M.A. (Ed.), Land Remote
764 Sensing and Global Environmental Change Remote Sensing and Digital Image Processing.
765 Springer, pp. 549–561.

766 Schimel, D., Hargrove, W., Hoffman, F., MacMahon, J., 2007. NEON: a hierarchically designed
767 national ecological network. Front. Ecol. Environ. 5, 59–59. doi:10.1890/1540-
768 9295(2007)5[59:NAHDNE]2.0.CO;2

769 Sellers, P.J., Meeson, B.W., Hall, F.G., Asrar, G., Murphy, R.E., Schiffer, R. a., Bretherton, F.P.,
770 Dickinson, R.E., Ellingson, R.G., Field, C.B., Huemmrich, K.F., Justice, C.O., Melack,
771 J.M., Roulet, N.T., Schimel, D.S., Try, P.D., 1995. Remote sensing of the land surface for
772 studies of global change: Models — algorithms — experiments. Remote Sens. Environ. 51,
773 3–26. doi:10.1016/0034-4257(94)00061-Q

774 Shuai, Y., Masek, J.G., Gao, F., Schaaf, C.B., 2011. An algorithm for the retrieval of 30-m
775 snow-free albedo from Landsat surface reflectance and MODIS BRDF. Remote Sens.
776 Environ. 115, 2204–2216. doi:10.1016/j.rse.2011.04.019

777 Shuai, Y., Masek, J.G., Gao, F., Schaaf, C.B., He, T., 2014. An approach for the long-term 30-m

land surface snow-free albedo retrieval from historic Landsat surface reflectance and MODIS-based a priori anisotropy knowledge. Remote Sens. Environ. 152, 467–479. doi:10.1016/j.rse.2014.07.009

Shuai, Y., Schaaf, C., Zhang, X., Strahler, A., Roy, D., Morisette, J., Wang, Z., Nightingale, J., Nickeson, J., Richardson, A.D., Xie, D., Wang, J., Li, X., Strabala, K., Davies, J.E., 2013. Daily MODIS 500 m reflectance anisotropy direct broadcast (DB) products for monitoring vegetation phenology dynamics. Int. J. Remote Sens. 34, 5997–6016. doi:10.1080/01431161.2013.803169

Vitasse, Y., Delzon, S., Dufr??ne, E., Pontailler, J.Y., Louvet, J.M., Kremer, A., Michalet, R., 2009. Leaf phenology sensitivity to temperature in European trees: Do within-species populations exhibit similar responses? Agric. For. Meteorol. 149, 735–744. doi:10.1016/j.agrformet.2008.10.019

Wang, Z., Schaaf, C.B., Chopping, M.J., Strahler, A.H., Wang, J., Román, M.O., Rocha, A. V., Woodcock, C.E., Shuai, Y., 2012. Evaluation of Moderate-resolution Imaging Spectroradiometer (MODIS) snow albedo product (MCD43A) over tundra. Remote Sens. Environ. 117, 264–280. doi:10.1016/j.rse.2011.10.002

Wang, Z., Schaaf, C.B., Strahler, A.H., Chopping, M.J., Rom??n, M.O., Shuai, Y., Woodcock, C.E., Hollinger, D.Y., Fitzjarrald, D.R., 2014. Evaluation of MODIS albedo product (MCD43A) over grassland, agriculture and forest surface types during dormant and snow-covered periods. Remote Sens. Environ. 140, 60–77. doi:10.1016/j.rse.2013.08.025

Woodcock, C.E., Strahler, A.H., Jupp, D.L.B., 1988a. The use of variograms in remote sensing: I. Scene models and simulated images. Remote Sens. Environ. 25, 323–348. doi:10.1016/0034-4257(88)90108-3

Woodcock, C.E., Strahler, A.H., Jupp, D.L.B., 1988b. The use of variograms in remote sensing: II. Real digital images. Remote Sens. Environ. 25, 349–379. doi:10.1016/0034-4257(88)90109-5

Zhang, X., Friedl, M. a., Schaaf, C.B., Strahler, A.H., Hodges, J.C.F., Gao, F., Reed, B.C., Huete, A., 2003. Monitoring vegetation phenology using MODIS. Remote Sens. Environ. 84, 471–475. doi:10.1016/S0034-4257(02)00135-9

Zhang, X., Friedl, M.A., Schaaf, C.B., 2006. Global vegetation phenology from Moderate Resolution Imaging Spectroradiometer (MODIS): Evaluation of global patterns and comparison with in situ measurements. J. Geophys. Res. G Biogeosciences 111. doi:10.1029/2006JG000217

Zhang, X., Wang, J., Gao, F., Liu, Y., Schaaf, C., Friedl, M., Yu, Y., Jayavelu, S., Gray, J., Liu, L., Yan, D., Henebry, G.M., 2017. Exploration of scaling effects on coarse resolution land surface phenology. Remote Sens. Environ. 190, 318–330. doi:10.1016/j.rse.2017.01.001

Zhu, X., Chen, J., Gao, F., Chen, X., Masek, J.G., 2010. An enhanced spatial and temporal adaptive reflectance fusion model for complex heterogeneous regions. Remote Sens. Environ. 114, 2610–2623. doi:10.1016/j.rse.2010.05.032

Zurita-Milla, R., Kaiser, G., Clevers, J.G.P.W., Schneider, W., Schaepman, M.E., 2009. Downscaling time series of MERIS full resolution data to monitor vegetation seasonal dynamics. Remote Sens. Environ. 113, 1874–1885. doi:10.1016/j.rse.2009.04.011

820